Water Research 297 (2026) 125770

Contents lists available at ScienceDirect

Water Research

journal homepage: www.elsevier.com/locate/watres

Critical degree of desalination (CDD), novel parameter for optimising the removal of ammonium ion from complex matrices in electrodialysis

Iosif Kaniadakis *, Zhenqiu Yang, Marianna Papadopoulou, Jules B. van Lier, Henri Spanjers

Delft University of Technology, Faculty of Civil Engineering and Geosciences, Stevinweg 1, 2628 CN, Delft, the Netherlands

HIGHLIGHTS

- Applying a critical degree of desalination (CDD) in electrodialysis (ED) achieves highest NH_4^+ removal efficiency for the lowest energy consumption.
- Monovalent CEM (mCEM) may not benefit ED for NH_4^+ removal from reject waters with molar fraction around 0.89.
- High concentration of K^+ can outcompete NH_4^+ removal in ED with mCEM.
- In sequence batch operation, the CDD allowed longer operation of the ED in a lower energy consumption.

GRAPHICAL ABSTRACT

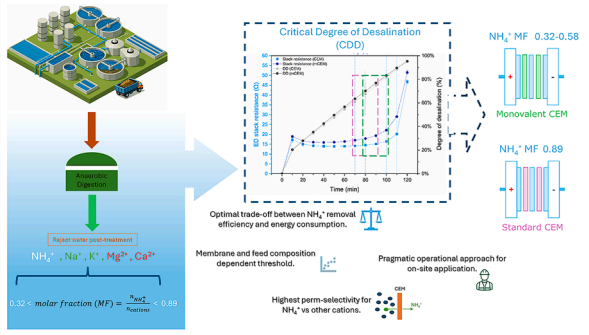

ARTICLE INFO

Keywords:
Cation competition
Cation-exchange membrane
Electrodialysis
Ammonium
Desalination

ABSTRACT

Complex waste streams, such as sludge reject water from anaerobic digestion, often contain a multitude of cations at varying concentrations, with the ammonium ion (NH_4^+) typically being the most abundant. Recently, electrodialysis (ED) has been developed as a technology for the removal and recovery of NH_4^+ from reject water. However, the further development of ED for targeting NH_4^+ recovery faces lack of reliable performance prediction and standardized operating strategies due to cation competition. It is postulated that selective rejection of divalent cations can be achieved through the use of monovalent-selective cation-exchange membranes (mCEMs). Due to their higher electrical resistance, questions remain regarding the cationic compositions under which mCEMs provide a substantial performance benefit. In the present study, three feed solutions simulating different molar cation compositions of reject water were subjected to ED using both mCEMs and conventional cation-exchange membranes (CEMs). The feed solutions were categorized based on the molar fraction of NH_4^+ relative to the total cation content. Results showed that the perm-selectivity of NH_4^+ over Mg^{2+} and Ca^{2+} was enhanced when using mCEMs. Moreover, mCEMs resulted in a higher overall NH_4^+ removal efficiency compared

Abbreviations: $E_{NH_4^+}$, Energy consumption for NH_4^+ transport ($MJ{\cdot}kgN^{-1}$); P_N^X, Perm-selectivity of cations X over NH_4^+; $RE_{\%}$, Removal Efficiency of NH_4^+; $\eta_{\%}$, Current efficiency for cation transport (%); AD, Anaerobic Digestion; AEEM, Anion-Exchange end Membrane; AEM, Anion-Exchange Membrane; BL, Boundary Layer; BPMED, Bipolar Membrane Electrodialysis; CDD, Critical Degree of Desalination (%); CEEM, Cation-Exchange End Membrane; CEM, Cation-Exchange Membrane; CP, Concentration Polarization; $DD_{\%}$, Degree of Desalination (%); ED, Electrodialysis; L_N, Load ratio; mCEM, Monovalent selective Cation-Exchange Membrane; MF, Molar Fraction; σ, Electrical conductivity ($mS{\cdot}cm^{-1}$).

* Corresponding author.
E-mail address: i.kaniadakis@tudelft.nl (I. Kaniadakis).

https://doi.org/10.1016/j.watres.2026.125770
Received 19 December 2025; Received in revised form 21 February 2026; Accepted 17 March 2026
Available online 18 March 2026

to standard CEMs. At a relatively low NH_4^+ molar fraction (0.32), mCEMs outperformed CEMs in terms of current efficiency. Notably, at an intermediate molar fraction (0.58), energy consumption was lower for mCEMs compared to CEMs, but only up to a critical degree of desalination (CDD). At a high molar fraction (0.89), the contribution of mCEMs was insignificant compared to that of CEMs. The CDD was identified as a pragmatic operational parameter beyond which further desalination leads to disproportionate energy penalties. For on-site-process-control of NH_4^+ removal with ED, the CDD demonstrated that membrane selection and operating thresholds are strongly dependent on reject water composition.

1. Introduction

1.1. Electrodialysis for NH_4^+ removal

Ammoniacal nitrogen (NH_4—N) is present in various municipal and industrial wastewater streams and poses a potential threat for the soil and aqueous environment when it is excessively discharged. Important sources of NH_4—N in wastewater streams are metabolic waste products, such as urea and mineralized proteins, next to agricultural runoffs and industrial processes in the food chain (Xiang et al., 2020). In contrast, NH_4—N is also considered a valuable resource, being an important component in fertilizers and other industrial products. In municipal wastewater treatment plants (WWTPs), sludge reject water after anaerobic digestion (AD) is considered an important contributor of NH_4—N in the wastewater (Deng et al., 2021). The concentration of NH_4—N in AD reject water often varies, depending on the exact WWTP layout and the type of sludge pre-treatment applied (Myllymäki et al., 2020). The most common form of aqueous ammoniacal nitrogen as a cation is NH_4^+. Nonetheless, NH_4^+ is the predominant cation in AD reject water, contributing significantly to its overall electrical conductivity (Deng et al., 2021). To reduce the concentration of NH_4^+ in the reject water prior its return to the WWTP headworks, different types of technologies have been developed such as biological autotrophic N removal (Deng et al., 2021). More recent developments focus on the removal but also on the recovery of NH_4^+ from reject waters, and make use of electrochemical techniques, such as electrodialysis (ED) and bipolar membrane electrodialysis (BPMED) (Ferrari et al., 2022)).

ED is an electrically-driven ion-exchange membrane process that has been extensively used to remove various ions, including NH_4^+, from various water and wastewater sources (Al-Amshawee et al., 2020; Bao et al., 2021). In an ED stack, cations and anions in the feed stream move in opposite directions due to the applied electric field. Cations pass through cation exchange membranes (CEM), while anions pass through anion-exchange membranes (AEM). In ED, ions are removed from the feed/ diluate solution to the concentrate solution (Strathmann, 2010). Previous research has shown that ED can yield high NH_4^+ removal efficiency exceeding 90%, when treating various types of wastewater, while concentrated NH_4^+ solutions are produced of at least 10 $g{\cdot}L^{-1}$ (Ippersiel et al., 2012). Another advantage of ED is the relatively low energy consumption ($E_{NH_4^+}$) for the removal of NH_4^+, especially from AD reject water, reaching values as low as 2–6 $kWh{\cdot}kgN^{-1}$ (Kaniadakis et al., 2024).

1.2. The challenge of selective removal of NH_4^+ with ED from streams with complex matrices

Reject water from AD often has substantial concentrations of K^+, Mg^{2+} and Ca^{2+}(Deng et al., 2021). Specifically, inorganic fouling or scaling can occur due to the presence of divalent and trivalent cations and a binding counter-ion even under moderate alkaline pH conditions (Ward et al., 2018). Inorganic fouling in ED systems is a challenge during treatment of streams with even negligible concentration of Ca^{2+} and Mg^{2+} cations in the feed (Rodrigues et al., 2020).

Literature research shows that mCEMs can effectively separate monovalent from divalent cations in complex ion-matrices, thereby preventing scaling (Ahdab et al., 2021; Ye et al., 2018). In our previous study we showed that monovalent selective cation exchange membranes (mCEMs) can be employed as an alternative to standard CEMs to reduce the transport of divalent or multivalent cations (Kaniadakis et al., 2024). In fact, a higher removal efficiency of NH_4^+ from real AD reject water was found (Kaniadakis et al., 2024). However, thus far it remains unclear when and to what extent the use of the more expensive mCEM is beneficial in comparison to standard CEMs in ED. In our current research we aimed to quantify the application potentials of mCEM for extracting NH_4^+ from complex matrices with the relative NH_4^+ concentration as a key parameter as explained in subsequent sections.

1.3. Adjusting the operational conditions in ED based on NH_4^+ feed concentration

Previous studies explored the optimal conditions for NH_4^+ removal and required energy input in electrochemical systems for scaled-up applications (Kuntke et al., 2018). To minimise excessive application of electric current in ED, Rodrigues Arredondo (2017) introduced the concept of load ratio (L_N). The L_N approach adjusts the applied current density in response to the NH_4^+ concentration in the feed stream, with the aim of characterising the current efficiency in ED. Since then, this metric has been employed in several studies to assess NH_4^+ removal efficiency in complex feed solutions (Rodrigues et al., 2023, 2020). In reject water, having a complex ion matrix, the total applied current is shared by all the present cations for their transport, influencing the overall current or transport efficiency. Because the composition of reject water varies per treatment site, NH_4^+ current efficiency is likely influenced differently across sites, even when applying the same L_N. According to (Rodrigues et al., 2020) the same L_N should yield similar removal efficiencies across feed streams with comparable molar fractions of NH_4^+ to all-cations. However, if two AD reject waters have the same NH_4^+ concentration but differ in concentrations of other cations the NH_4^+ current efficiency will differ. Most recent studies have focused only on a single molar fraction (NH_4^+:all-cations) of reject water (Kaniadakis et al., 2024; Yang et al., 2023). Other recent studies applied the L_N in a BPMED pilot to remove NH_4^+ from real sludge reject water after AD, having different compositions (Ferrari et al., 2022; Rodrigues et al., 2023). However, the results on current efficiency and removal efficiency varied, albeit the same L_N was applied in these studies, targeting different wastewater compositions. Thus far, the effect of different cation molar fractions in AD reject water on ED performance, targeting a specific removal efficiency, has not been explored.

1.4. Performance characterization for NH_4^+ removal in ED

ED performance characterization relies on key variables, such as L_N and limiting current density (LCD), which serve as important process settings for optimizing NH_4^+ removal and minimizing energy consumption in wastewater treatment (Rodríguez Arredondo et al., 2017;). These key variables have been used to set a balance between highest removal efficiency and lowest possible energy consumption.

Ward et al. (2018) operated an ED pilot for NH_4^+ removal from AD sludge reject water under 60–80% of the LCD, demonstrating effective ammonium removal within specific energy consumption targets. Two studies on ED (Ippersiel et al., 2012; Mondor et al., 2008) used the degree of desalination for setting a threshold to the stack resistance in

batch ED operations, reporting an optimum of 80% desalination. Van Linden et al. (2019) investigated a dynamic control approach by adjusting the applied LCD according to electrical conductivity trajectories, specifically targeting NH_4^+ as the principal cation. Prior studies typically investigate ED performance under a single molar fraction (MF) of cation composition, without accounting for the variability found in real AD reject waters. Consequently, reported values for NH_4^+ current efficiency, removal efficiency, and energy consumption are often inconsistent across the literature. Since NH_4^+ concentrations in AD reject waters fluctuate due to site-specific treatment processes, categorizing reject waters solely by NH_4^+ levels or electrical conductivity proves insufficient (Pavez-Jara et al., 2023). Therefore, a more robust approach is to categorize reject water based on the overall cationic makeup expressed as a molar fraction to systematically evaluate membrane performance and cation selectivity under realistic and varying conditions.

A recent study on electrodialysis of AD reject water demonstrated that operation under a constant applied potential of 30 V promotes preferential NH_4^+ transport over competing cations, while divalent species exhibit delayed transport relative to monovalent ions, consistent with selective ion permeation behavior (Proskynitopoulou et al., 2024). In an ED pilot study, segmentation of the operational time was demonstrated as an effective strategy for optimizing the energy consumption associated with NH_4^+ and K^+ recovery (Xiao et al., 2023). However, the aforementioned approaches do not explicitly account for the influence of varying cationic matrices.

1.5. Research objective

Research focusing on NH_4^+ recovery from AD reject waters with ED and BPMED is a recent and novel strategy (Meng et al., 2024). Most approaches, however, disregarded the impact of competing cations on NH_4^+ current efficiency, energy consumption and removal efficiency. Moreover, the influence of mCEMs in ED performance in multiple AD reject water compositions is not fully explored. Based on literature and the analysis of reject water samples, we categorized the cation composition profiles of reject water into three main molar fractions (MFs), focusing on the five primary cations: K^+, Na^+, Ca^{2+}, Mg^{2+}, and NH_4^+ present in AD reject water. Furthermore, standard CEMs and mCEMs in ED were tested to evaluate the effectiveness of mCEMs under different reject water composition. It is anticipated that NH_4^+ removal efficiency and cation perm-selectivity through standard and monovalent selective cation-exchange membranes may vary across different MFs. Additionally, this study aimed to identify the optimal operational values for ED based on the critical degree of desalination (CDD) for the highest NH_4^+ removal efficiency, while avoiding excessive stack resistance escalation. Finally, the impact of composition on the performance of ED is extensively discussed in this study. To the best of our knowledge, this is the first study to present a lab-scale framework for understanding how different cation-compositions in AD reject water affect NH_4^+ perm-selectivity, removal efficiency, current efficiency and energy consumption in ED.

2. Materials and methods

2.1. Experimental setup

Fig. 1 shows a schematic representation of the experimental setup. The tested ED cell was designed and supplied by RedStack B.V. (Sneek, The Netherlands). The electrodes of the cathode and the anode were Pt-Ir coated of metal-stretched TiO_2 with an active surface area of 10 cm x 10 cm. A programmable power supply (Tenma 72–2535) was used to apply electrical current with range of 0.001 to 3.000 Amperes (A) and voltage of 0.010 to 30.000 Volts (V). The electrical current and voltage were logged every two seconds, and the output data were automatically stored. The electrical conductivity and pH of the solutions were measured in their respective stirring bottles using one WTW Multi 3630 IDS multi-meter with two calibrated TetraCon 925 electrical conductivity sensors and two calibrated IDS SenTix 940 pH sensors. Magnetic stirrers were placed inside the bottles of diluate, concentrate, and electrode rinse solution (ERS) to ensure homogeneous mixing. As ERS, an aqueous solution of 20 $g{\cdot}L^{-1}$ Na_2SO_4 was made. The diluate and concentrate solutions were recirculated through the membrane stack at a cross-flow velocity of 2 $cm{\cdot}s^{-1}$ by calibrated Masterflex® L/S®

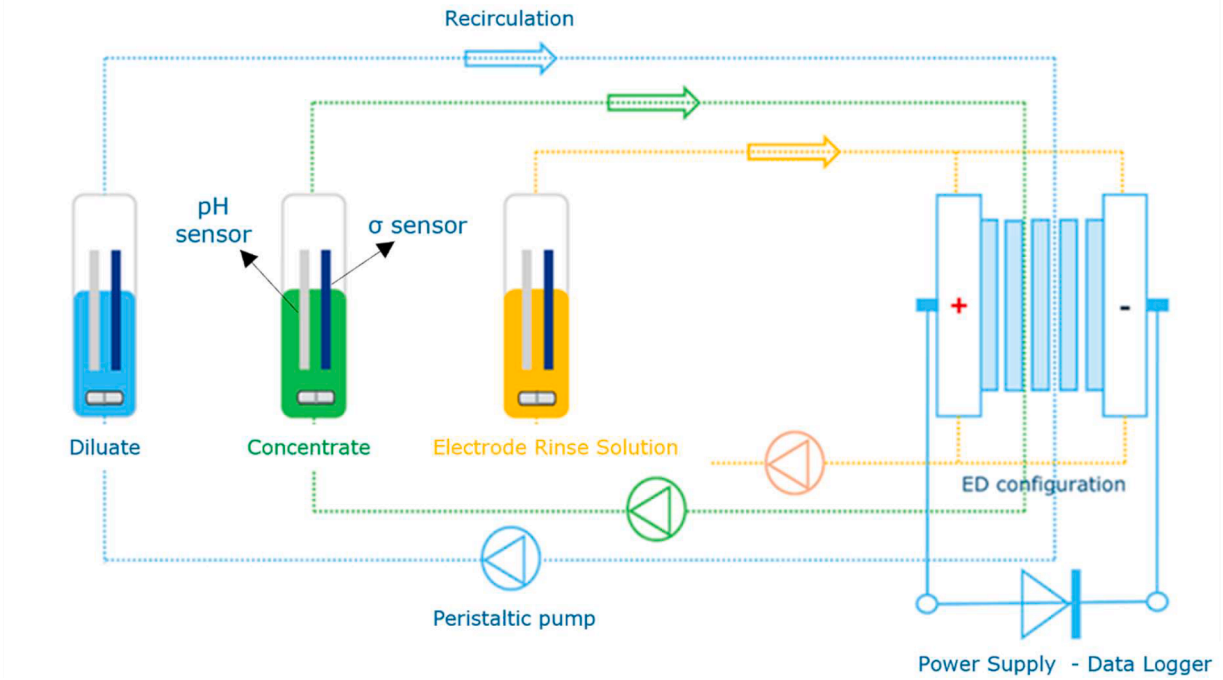

Fig. 1. The experimental set-up, including the ED cell, the power supply with data logger, the three pH and σ sensors, the three peristaltic pumps, and the vessels for diluate, concentrate, and ERS solutions recirculating through the ED cell.

peristaltic pump (Strathmann, 2010; van Linden et al., 2020). A calibrated peristaltic Watson-Marlow 520S pump was used to recirculate the solutions in the ED stack at a flow rate of 19 $L \cdot h^{-1}$.

2.2. Membrane configuration

The stack shown in Fig. 2(a) was designed with five pairs of FAS-PET-130 anion exchange membranes (AEMs) and five FKS-50 cation exchange membranes (CEMs). To minimize NH_4^+ leakage into the electrode rinse solution (ERS), restrict the Na^+ leakage to the diluate, and to reduce the NH_4^+ transport only through the CEM/mCEM two AEMs were positioned as anion exchange-end membranes (AEEMs) adjacent to the electrode chambers. Previous studies (van Linden et al., 2020; Yang et al., 2023) demonstrated that placing AEEMs next to electrode chambers significantly reduced NH_4^+ leakage, with Yang et al. (2023) reporting nearly twice the final NH_4^+ concentration in the ERS in configurations with AEEMs compared to cation end-exchange membranes (CEEMs). Therefore, AEEMs effectively retain NH_4^+ ions, preventing their migration into the ERS and improved NH_4^+ tracing through the stack. To form the diluate and concentrate chambers, wire mesh spacers made of silicon/polyethylene (0.27 mm thickness) were used to separate each AEM and CEM, allowing for a thinner boundary layer (BL) and lower resistance as achieved with spacers of 0.5 mm (Vermaas et al., 2014). For the stack in Fig. 2(b), the CEMs were replaced by monovalent-selective CEMs (mCEMs) from Astom, Japan, whereas AEMs and AEEMs remained the same.

The mechanical and electrical characteristics of the chosen membranes are presented in Table 1. It is expected that mCEM could result in higher stack resistance based on the values of membrane resistance and thickness. The CIMS membrane is approximately three times thicker than the FKS-50 membrane due to an additional monovalent-selective layer on one side, which was oriented toward the diluate in the stack[b].

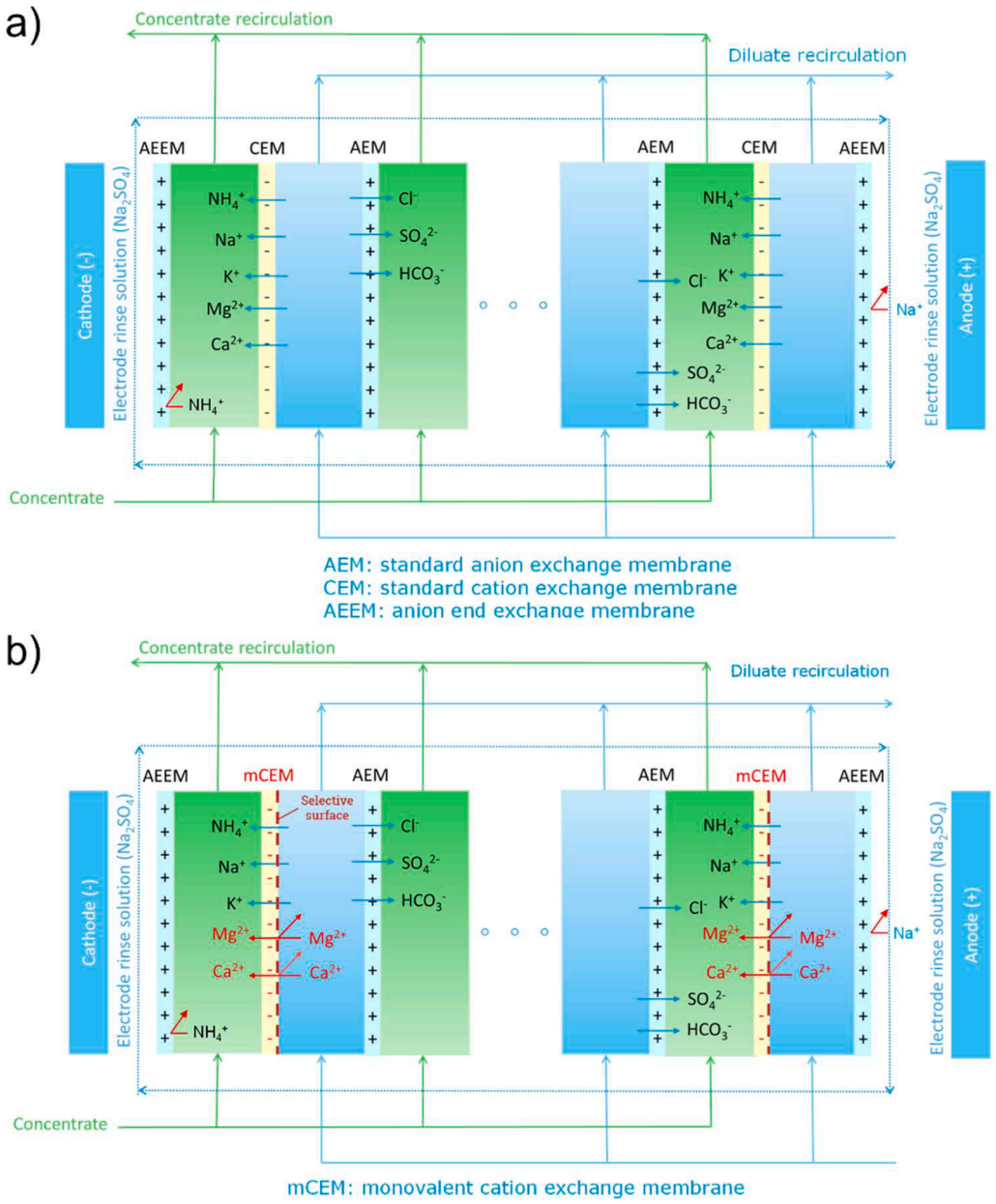

Fig. 2. The two tested configurations of ED stacks with CEM (a) and mCEM (b). The purpose of incorporating mCEMs in ED (b) is to reduce the transport of Mg^{2+} and Ca^{2+} as illustrated by red arrows. The monovalent-selective one side surface of the mCEM is indicated with red dashed line. The incorporation of AEEM is depicted restricting the NH_4^+ migration into the ERS Na^+ leakage.

Table 1
Membrane specifications as described by manufacturers Fumatech[a] and ASTOM[b] and (Wang and Lin, 2024).

Type	Name	Specific resistance (Ω cm^2)	Thickness (mm)	Conductivity (mScm^{-1})	Perm-selectivity[a, b]
CEM[a]	FKS-50	1.8–2.5	0.05	2–3	>97%
mCEM[b]	CIMS	2–2.5	0.15	N/A	>98%
AEM[a]	FAS-PET-130	1.7–3	0.1–0.13	4–6	>92%

2.3. Experimental methodology

2.3.1. Single batches with synthetic solutions

The MF values listed in Table 2 were calculated based on reject water samples from WWTPs in the Netherlands from the sites of Sluisjesdijk, Olburgen, Tilburg, Hengelo, Apeldoorn, Amersfoort, Venlo, and Horstermeer, but also from existing literature (El-Qelish and Mahmoud, 2022; Koskue et al., 2021a, 2021b; Shaddel et al., 2020a, 2020b). Based on these calculations, the obtained MFs were 0.32 as the most complex, to 0.89 as the least complex AD reject water composition. Subsequently, the MF of 0.58 was defined as an estimation of the total average. Additionally, the molar concentration of NH_4^+ was kept constant across all MF to enable fair comparisons and minimize the impact of concentration variations on performance indicators among the experiments. In this study, the NH_4^+ concentration in all samples was standardized to 1000 mg·L^{-1} whereas the proportions of the rest of the cations were adjusted to achieve the specific molar fraction number.

Eq. (1) defines the calculation used to determine the molar fraction presented in Table 2.

$$molar\ fraction\ (MF) = \frac{n_{NH_4^+}}{n_{cations}} \quad (1)$$

Where $n_{NH_4^+}$ is the added amount of NH_4^+ in moles, and $n_{cations}$ is the summation of all cations in the solution in moles, including NH_4^+, Na^+, K^+, Mg^{2+}, and Ca^{2+}. The synthetic feed solutions initially contained the corresponding salt weight of ammonium bicarbonate (NH_4HCO_3), sodium sulfate (Na_2SO_4), potassium bicarbonate ($KHCO_3$), magnesium chloride ($MgCl_2$), calcium chloride ($CaCl_2$) in 1 L of demi water (Table 2). The initial concentrate solution was 1 L demi water. Samples were taken from diluate and concentrate solutions at various time instants until the batch experiments were completed. During the experiment applying an MF of 0.32, the samples were taken every 20 s from the diluate and concentrate solution. Using an MF of 0.58 and 0.89, the samples were taken every 10 s from both solutions. Subsequently, NH_4^+, Na^+, K^+, Mg^{2+}, and Ca^{2+} concentrations were measured using an ion chromatograph (ICS-2100, Thermo Scientific Dionex, USA) equipped with an analytical column (IonPac AS17-C 2 mm, Thermo Scientific Dionex, USA) and an electrical conductivity sensor. The experiments were all performed in duplicate at 20 ± 1 °C in the lab. Furthermore, the water volumes of the solutions remained the same during the experiments indicating that the electro-osmotic transport of water was minimum. For these experiments the iron species of Fe^{2+}/Fe^{3+}, present in AD, were eliminated from the scope of the study. The reason lies under the potency of these cations to cause irreversible membrane degradation of the CEM surface especially in high concentrations (Chen et al., 2017). Furthermore, trivalent cations do not compete directly with NH_4^+ in electrodialysis as divalent cations due their limited mobility through the membrane and therefore they were not included (Lambert et al., 2006; Sadrzadeh et al., 2007)

Table 2
Composition of the used media simulating the cation composition of the different reject waters, based on molar fractions (MFs) observed at wastewater treatment sites in the Netherlands.

Cation molar concentration (mM)					
Solutions	NH_4^+	Na^+	K^+	Mg^{2+}	Ca^{2+}
MF = 0.32	55.44	11.06	83.87	21.00	3.37
MF = 0.58	55.44	3.92	14.83	19.75	1.16
MF = 0.89	55.44	3.12	2.23	0.27	0.96

2.3.2. Sequential batch experiments with real reject water

To test the relevance of the observed inflection time of critical degree of desalination (CDD) for real-world conditions, sequential batch experiments (SBEs) were performed using ED equipped with both types of membranes on real reject water. A sample of real AD reject water was collected from the wastewater treatment plant of Horstermeer in the Netherlands. The cation composition was analyzed with ion-chromatography and the calculated MF was 0.52. Therefore, the reject water composition was approached similarly to MF 0.58 for both membranes. The experiments were terminated once the concentrate solution reached the electrical conductivity of 20 mS·cm^{-1}.

2.4. Performance indicators

The NH_4^+ removal efficiency ($RE_{\%}$) was calculated using Eq. (2):

$$RE_{\%} = \frac{C_{d,0}^N - C_{d,t}^N}{C_{d,0}^N} \cdot 100\% \quad (2)$$

where $C_{d,t}^N$ and $C_{d,0}^N$ are concentrations of NH_4^+-N in the diluate solution at time t and 0, respectively.

The total cumulative energy consumption ($E_{NH_4^+}$) expressed in MJ·kgN^{-1} for the mass of removed NH_4^+ was calculated using Eq. (3).

$$E_{NH_4^+} = \frac{\sum_{t=0}^{t}(U_t \cdot I_t \cdot \Delta t)}{mNH_4^+, d} \quad (3)$$

where $E_{NH_4^+}$ is the energy consumption (in MJ·kgN^{-1}), U_t is the average electric potential during each time interval (in V), I_t is the average electric current during a time interval (in A or C · s^{-1}) and Δt is the time interval (in seconds), and mNH_4^+, d is the mass of NH_4^+ transported from the diluate.

The degree of desalination (%) was calculated using Eq. (4).

$$Degree\ of\ Desalination\ (DD_{\%}) = \left(1 - \frac{\sigma_t}{\sigma_0}\right) \cdot 100\% \quad (4)$$

Where σ_t (mS·cm^{-1}) is the electrical conductivity of diluate solution at time t, and σ_0 (mS·cm^{-1}) is the initial electrical conductivity of diluate solution.

The current efficiency ($\eta_{\%}$) of cation species i was calculated using Eq (5).

$$\eta_{\%} = \frac{\left(C_{c,t}^i - C_{c,0}^i\right) \cdot V_d \cdot F \cdot z_i}{N \cdot A \cdot t \cdot I_d} \cdot 100\% \quad (5)$$

where $C_{c,\tau}^i$ and $C_{c,0}^i$ are molar concentrations of the cations i in the concentrate solution at time t and 0, respectively; V_d is the volume of diluate solution; F is the Faraday constant (96,485 C·mol^{-1}); z_i is the valence of the species i; N is the number of cell pairs in the ED stack (dimensionless, $N = 5$); A is the effective area of each membrane (m^2); Δt is the time (s); I_d is the current density (A·m^2).

The fraction in moles of each ion that migrated from the diluate to the concentrate relative to their initial concentration was used to express the perm-selectivity of CEM and mCEM for Na^+, K^+, Mg^{2+}, and Ca^{2+} indicated as X with respect to NH_4^+ (P_N^X) (Van der Bruggen et al., 2004):

$$P_N^X = \frac{[(C_t^X - C_0^X)\cdot V_c]/[(C_t^N - C_0^N)\cdot V_c]}{C_0^X/C_0^N} = \frac{(\eta_{X,\%}/z_X)/(\eta_{N,\%}/z_N)}{C_0^X/C_0^N} \quad (6)$$

where C_t^X and C_t^N are the molar concentrations of X cation and NH_4^+ at a specific time instant, respectively, $\eta_{X,t}$ and $\eta_{N,t}$ are the current efficiencies of X cation and NH_4^+ transported from the diluate to the concentrate chamber at time instant t, respectively, V_c is the volume of the concentrate, z_X and z_N are the ionic charges of X cation and NH_4^+, respectively. When $P_N^X > 1$, the membrane is more selective to X cation than NH_4^+ while for $P_N^X < 1$, the membrane is more selective to NH_4^+ than X cation.

2.5. Statistical analysis

Statistical analysis on the measured data was performed using IBM SPSS Statistics software. The following statistical tests were used to analyze the data and support the interpretation of the results: Piecewise linear regression and ANOVA (to evaluate increasing or decreasing trends), and *t*-test on linear regression slopes (to assess significant changes in slope). The error bars in the figures present the maximum and minimum values (i.e. outer values of error bars).

3. Results and discussion

3.1. Molar fraction 0.32: reduced NH_4^+ current efficiency for the most complex ion composition

Fig. 3(a) and (b) compare the $\eta_{\%}$ of the five key cations at a MF of 0.32 for both membranes. The highest $\eta_{\%}$ was observed at the beginning of the experiment, indicated as phase I.

During phase I, the $\eta_{\%}$ was driven by the high concentration gradient between the diluate and concentrate solutions (van Linden et al., 2020, 2019). As a result, the sum of $\eta_{\%}$ for all the cations exceeded 100% indicating the existence of additional transporting driving force other than electric current, as previously demonstrated by others (Rodríguez Arredondo et al., 2019). After the ion distribution equilibrated and the influence of concentration gradient diminished, the sum of $\eta_{\%}$ approached 100%, which was marked as entering phase II, during which the transport of cations occurred primarily by electro-migration.

At MF 0.32, K^+ emerged as the primary charge carrier due to its high feed concentration and high electro-mobility. As a result, the $\eta_{\%}$ for K^+ was higher than for NH_4^+. The transport of K^+ was enhanced with mCEM when compared to CEM, as reflected by the average $\eta_{\%}$ of 67% ± 3% and 50% ± 1%, respectively. Due to the high abundance of K^+, the $\eta_{\%}$ of NH_4^+ was the lowest among the experiments. Nevertheless, the average $\eta_{\%}$ for NH_4^+ for the total batch duration was 40% ± 1% with mCEM and 35% ± 2% with CEM, meaning that the monovalent selective property of mCEM improved the transport of both K^+ and NH_4^+.

Mg^{2+} exhibited a distinct $\eta_{\%}$ trend compared to the other cations across the two membranes. The total $\eta_{\%}$ for Mg^{2+} was 20% ± 2% and 25% ± 1% for mCEM and CEM, respectively. In mCEM, the transport of Mg^{2+} was limited especially during the first 60 min showing a delayed increase ($\rho = 0.99$, $p < 0.001$) at 50% $DD_{\%}$. Notably, after 75% $DD_{\%}$, Mg^{2+} and NH_4^+ transport converged in the CEM, indicating a clear competition between these ion species at $DD_{\%}$ exceeding 75%.

Fig. 3(c), (d), and (e) further examine the perm-selectivity (P_N^X) at 50%, 75%, and 95% $DD_{\%}$ for both membranes. The results demonstrated that the mCEM rejected more effectively Mg^{2+} and Ca^{2+} compared to

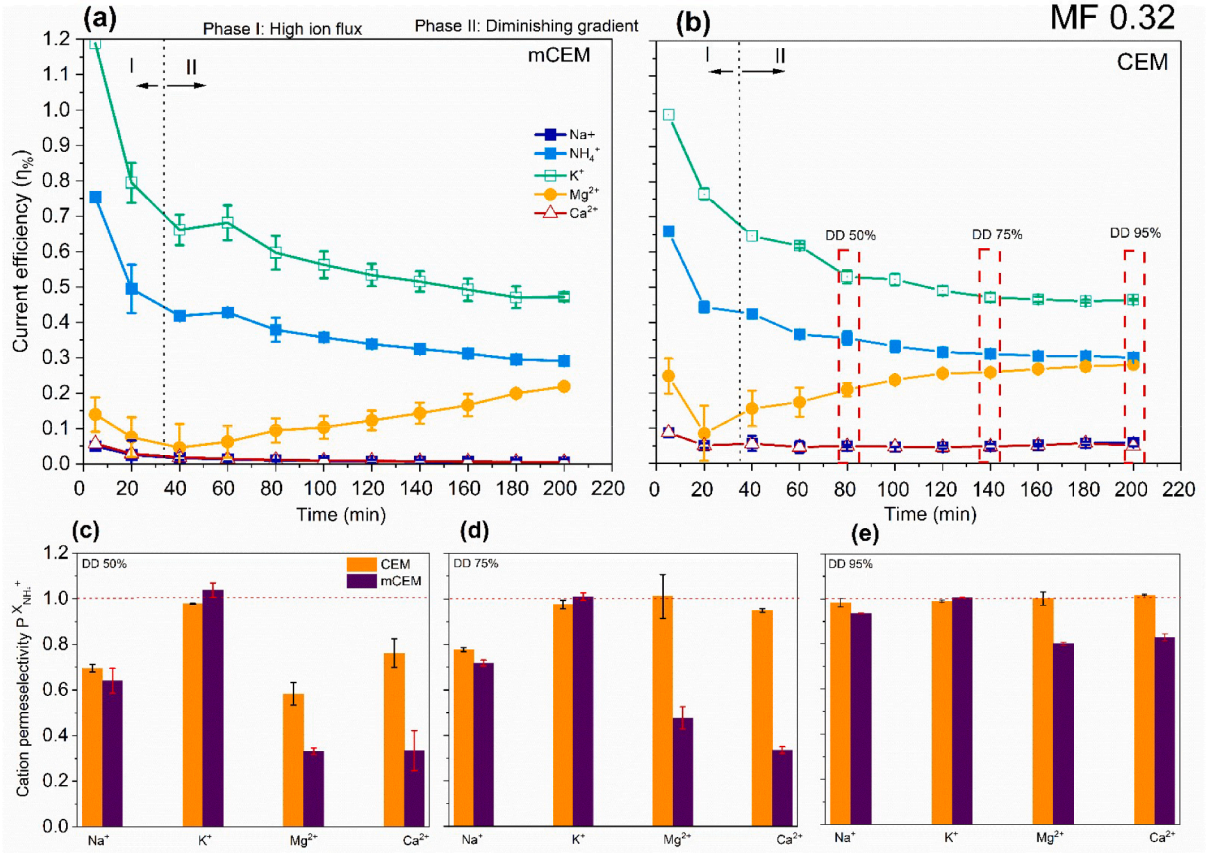

Fig. 3. The current efficiency as a function of time of each cation for mCEM (a) and CEM (b). The cation perm-selectivity of the different cations over NH_4^+ for both mCEM and CEM at $DD_{\%}$ 50% (c), 75% (d) and 95% (e). MF 0.32: molar fraction of 0.32, $DD_{\%}$: degree of desalination, $\eta_{\%}$: current efficiency, P_N^X membrane perm-selectivity of cation X over NH_4^+. Phase I reflects the combined effects of diffusion and electromigration, whereas phase II indicates a diminished diffusion influence with predominant electromigration.

CEM. Accordingly, the CEM showed a higher P_N^X for divalent cations than mCEM, particularly at 75% DD%. Notably, Na^+ and K^+ exhibited similar patterns in selectivity for both membranes, across the tested DD%. The P_N^X of mCEM for monovalent cations and therefore for NH_4^+ approached 1, indicating an equal selectivity with divalent cations at DD% exceeding 75%, following the same trend of $\eta_{\%}$.

3.2. Molar fraction 0.58: superior performance of mCEM over CEM on selective NH_4^+ transport

Fig. 4(a) and (b) show the $\eta_{\%}$ during the experiment with MF of 0.58. The average $\eta_{\%}$ of NH_4^+ was 67% ± 2% and 54% ± 1% for mCEM and CEM, respectively, indicating that mCEM yielded a higher $\eta_{\%}$ for NH_4^+. Regarding the transport of Mg^{2+} the average $\eta_{\%}$ was 26% ± 3% and 39% ± 2% for mCEM and CEM, respectively. Therefore, the transport of Mg^{2+} was limited by the mCEM. Notably, the slope of Mg^{2+} shifted direction and showed an increase at approximately 50% DD% ($p < 0.001$). In CEM, Mg^{2+} and NH_4^+ showed a similar decreasing trend (ρ=−0.9,$p = 0.002$) throughout the experiment. However, a broader disparity was observed in mCEM than CEM in $\eta_{\%}$ between NH_4^+ and Mg^{2+}. The $\eta_{\%}$ of K^+ was 25% ± 3% and 13% ± 3% for the mCEM and CEM, respectively, indicating that the monovalent selective layer favoured the transport of K^+.

Fig. 4(c), (d), and (e) show P_N^X of both membranes at 50%, 75%, and 95% DD%. The results indicate that the mCEM yielded a higher selective transport of NH_4^+, while the CEM showed greater preference for Mg^{2+} and Ca^{2+} at every DD%. The P_N^X of mCEM for divalent cations was constantly below 1. Like the $\eta_{\%}$ trends, mCEM showed a delayed increase in the migration of the divalent cations, while NH_4^+ migration dominated earlier, which led to higher P_N^X for divalent cations at higher DD%. Obtained results suggested a transition from monovalent to divalent selectivity at higher DD%.

We can conclude that for an MF of 0.58, the mCEM configuration represented a superior alternative for the enhancement of NH_4^+ transport compared to CEM configuration. The cation selectivity of transported cations from the diluate solution was: $Mg^{2+} \approx Ca^{2+} > K^+ \approx NH_4^+ > Na^+$ for CEM configuration and $NH_4^+ > K^+ > Na^+ > Ca^{2+} > Mg^{2+}$ for mCEM configuration.

3.3. Molar fraction 0.89: highest NH_4^+ $\eta_{\%}$ due to low concentration of competing cations and minimum improvement by the mCEM

Fig. 5(a) and (b) depict the $\eta_{\%}$ for all cations during the experiment with MF 0.89 for mCEM and CEM respectively. The highest $\eta_{\%}$ was observed during the first 20 mins of operation, during phase I. Overall, there was no significant improvement to the $\eta_{\%}$ of NH_4^+ by the mCEM when compared to CEM (t= −0.61 $p = 0.27$). Regarding P_N^X, Fig. 4(c), (d) and (e) show that the CEM was more selective towards divalent cations compared to experiments applying lower NH_4^+MFs, especially at DD% above 50% and 75% and despite the lowest concentration of these competing cations. Concentration polarization (CP) is characterized by a

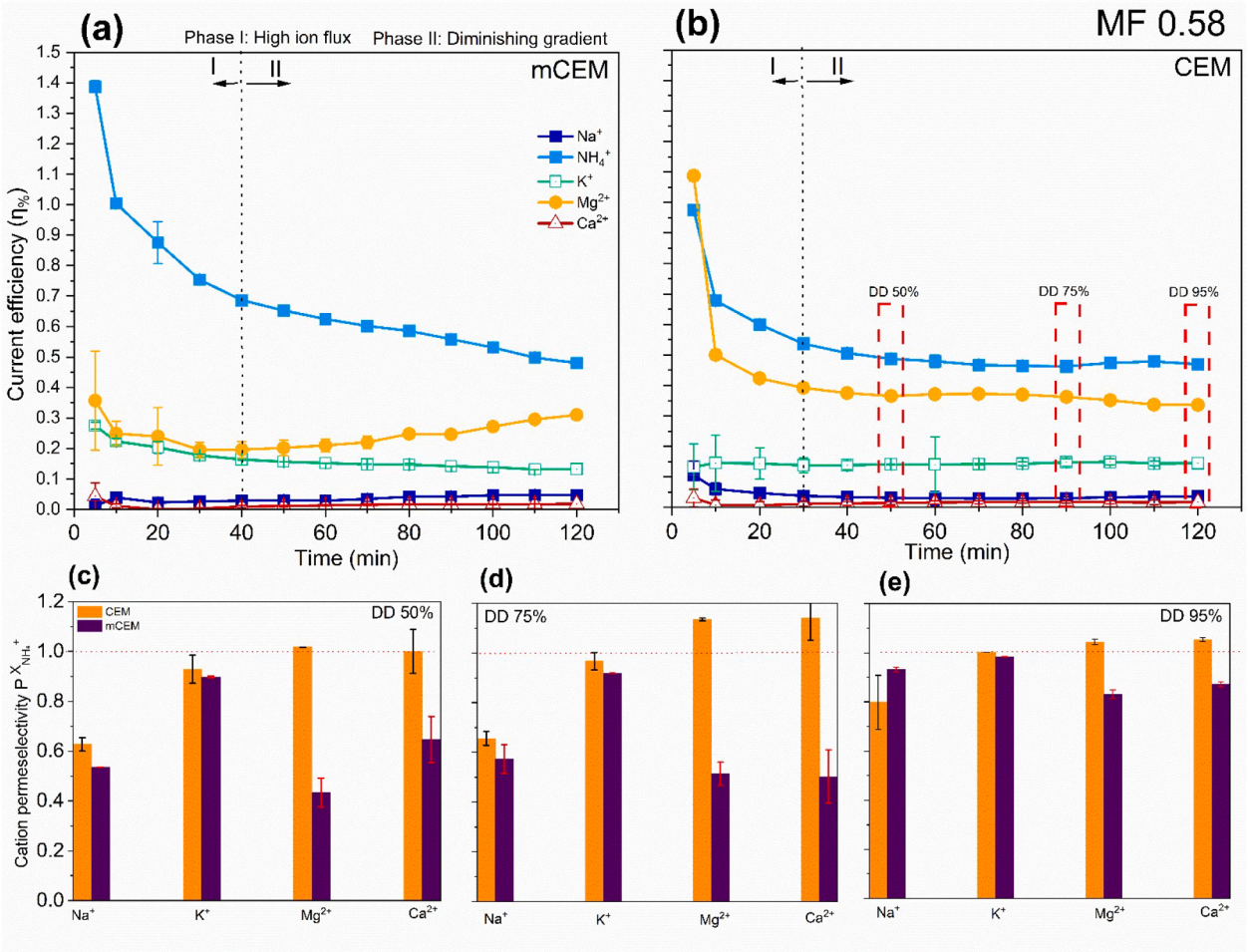

Fig. 4. The current efficiency as a function of time of each cation for mCEM (a) and CEM (b). The cation perm-selectivity over NH_4^+ (P_N^X) for both mCEM and CEM at DD% 50% (c), 75% (d) and 95% (e). MF 0.58: molar fraction of 0.58, DD%: degree of desalination, $\eta_{\%}$: current efficiency, P_N^X membrane perm-selectivity of cation X over NH_4^+.

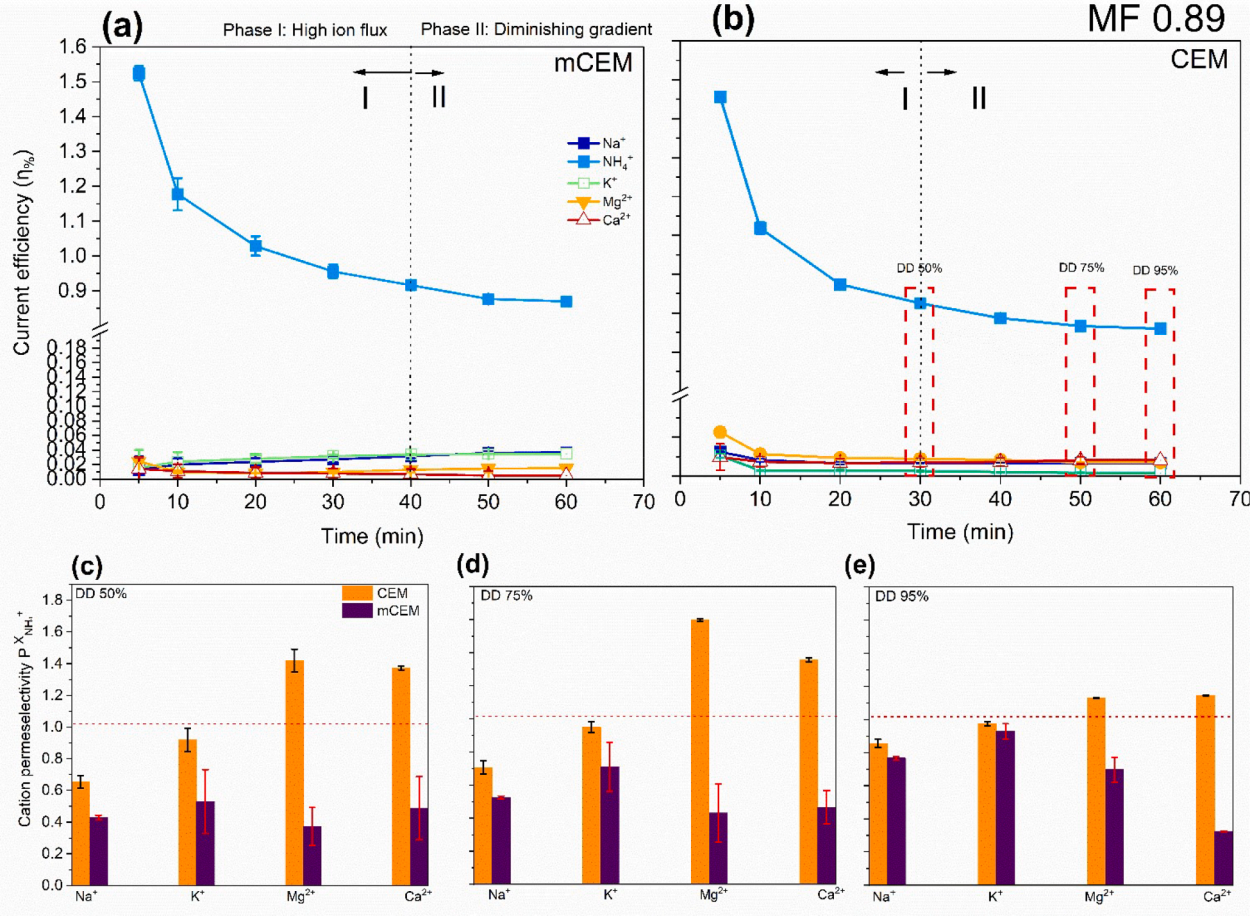

Fig. 5. The current efficiency as a function of time of each cation for mCEM (a) and CEM (b). The cation perm-selectivity over NH_4^+ (P_N^X) for both mCEM and CEM in $DD_{\%}$ 50% (c), 75% (d) and 95% (e). MF 0.89: molar fraction of 0.89, $DD_{\%}$: degree of desalination, $\eta_{\%}$: current efficiency, P_N^X membrane perm-selectivity of cation X over NH_4^+.

higher concentration of ions in the BL of the membrane than in the bulk indicating limiting current conditions (Tanaka, 2003). Obtained findings suggested that low concentrations of divalent cations resulted in high $\eta_{\%}$ for NH_4^+ transport. Possibly this is linked to reduced CP at the BL, owing to a reduced thickness and thus increased diffusivity of NH_4^+ ions. This assumption is in line with the hypothesis that the concentration profile towards the membrane surface becomes steeper (Kim et al., 2012; Shocron et al., 2025). The total P_N^X values for each conditions before the critical point are shown in Table S3.

The observed differences in P_N^X between the mCEM and CEM at MF 0.32 and 0.58 follow the behaviour predicted by theory, as described by Kim et al. (2011) and demonstrated experimentally by Roghmans et al. (2020). At current densities lower or close to the limiting current density, stronger concentration polarization of multivalent ions in the boundary layer governs membrane perm-selectivity, as the monovalent cations were depleted first from the bulk (Table S2). According to (Firdaous et al., 2007), the composition of the feed solution, considering the valence and concentration of cations, can influence the diffusive BL of a CEM in ED. Specifically, the phenomenon of CP can become more important, when applying a more complex solution of multivalent cations. In Fig. 3(a), (b) and Fig. 4(a),(b) NH_4^+ $\eta_{\%}$ showed a decreasing trend indicating a simultaneous depletion of NH_4^+ concentration from the bulk. However, Mg^{2+} in mCEM showed an increasing $\eta_{\%}$ trend at $DD_{\%}$ exceeding 50%. The observed trend was attributed to the effect of the mono-selective mCEM polymer-chemistry and resulted in a prioritized transport of monovalent cations in the first period of the experiment. After the NH_4^+ concentration in the BL dropped below a critical point, Mg^{2+} started diffusing from the bulk solution into the BL, demonstrating competition for transport sites. Results in Fig. 3(b) indicated that Mg^{2+} migration was triggered earlier compared to Fig. 3(a). However, the presence of both monovalent and divalent cations in the BL of a selective membrane can lead to electrochemical blocking of the pore sites by the latter, due to their larger radius and higher charge (Firdaous et al., 2007; Rodrigues et al., 2022). Therefore, by using an mCEM the transport of monovalent cations over divalent was indeed favoured, although a thicker diffusive BL and a more intensified CP occurred (Al-Amshawee et al., 2020; Kim et al., 2011). Additionally, the different structure of the selective chemistry of mCEM could have potentially affected the thickness and the concentration profile of the BL (Kim et al., 2012; Yang et al., 2023). A selective fabricated layer of the same type of mCEM reduces the transport of cations with larger hydrated radii such as $Ca^{2+}$and Mg^{2+}according to (Zimmermann et al., 2024). As a result, an exclusion mechanism of a smaller porosity contributed to higher selectivity by the current mCEM based on (Roghmans et al., 2020).

At MF 0.89, the CEM showed the highest selectivity for divalent cations despite their very low concentration. It is assumed that $Ca^{2+}$and Mg^{2+} were attracted with higher affinity to the pore sites due to their higher charge density.

3.4. NH_4^+ removal efficiency and energy consumption depend on the degree of desalination

In Fig. 6(a), (b) and (c) the $RE_{\%}$ for different $DD_{\%}$ is shown for MF 0.32, 0.58 and 0.89, respectively. The highest $RE_{\%}$ of applying a CEM

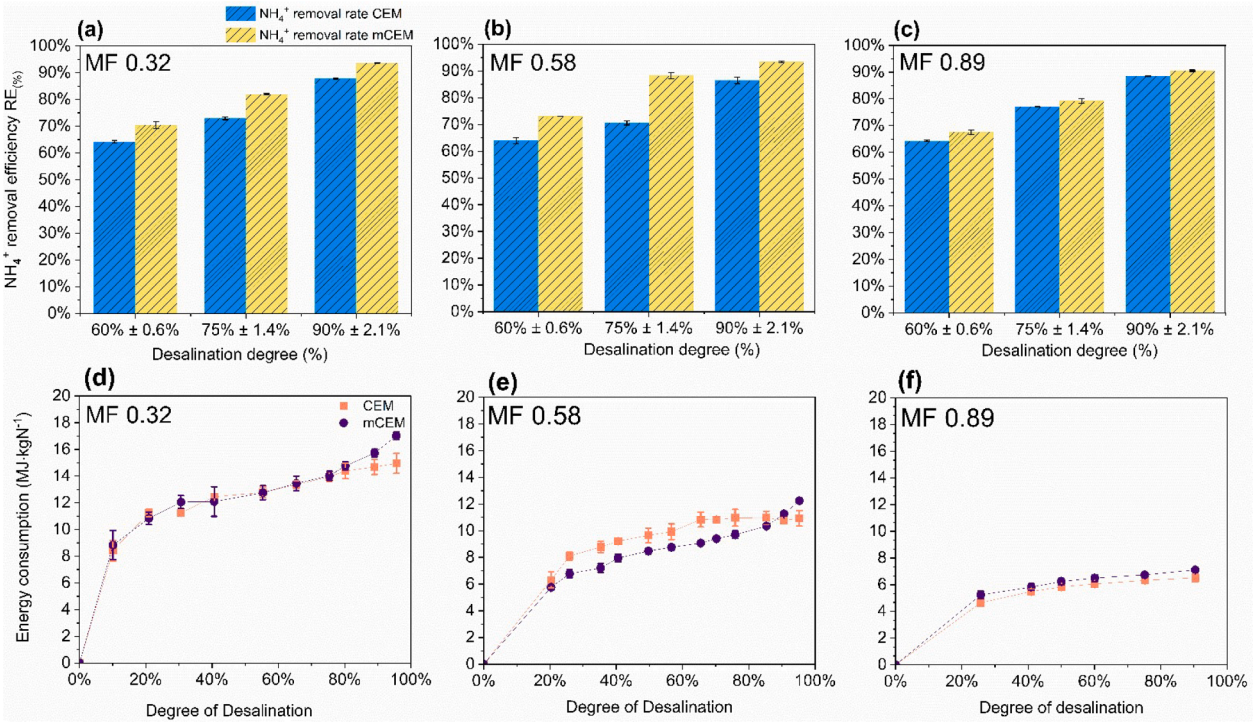

Fig. 6. The $RE_{\%}$ of NH_4^+ for mCEM (yellow) and CEM (blue) at different $DD_{\%}$ for MF 0.32 (a), MF 0.58 (b), and MF 0.89 (c). The energy consumption ($MJ{\cdot}kgN^{-1}$) as a function of $DD_{\%}$ for mCEM (purple) and CEM (orange) at MF 0.32 (d), MF 0.58 (e), and MF 0.89 (f). $RE_{\%}$: removal efficiency, $DD_{\%}$: degree of desalination, MF: molar fraction.

was obtained for MF 0.89 at $DD_{\%}$ 90% (Fig. 6(c)), and the lowest for MF 0.32 at $DD_{\%}$ 60% (Fig. 6(a)). The mCEM achieved the highest $RE_{\%}$ for all MFs and for all three corresponding $DD_{\%}$ compared to the CEM (Fig. 6 (b)). More specifically, the mCEM improved the $RE_{\%}$ in MF 0.58 at 75% $DD_{\%}$ by 18%, while the lowest improvement was observed with MF 0.89. In addition, under the latter conditions the improvement was almost negligible (Fig. 6(c)). For MF 0.32, the primary challenge was the dominance of K^+, due to its higher concentration and mobility, which influenced negatively the NH_4^+ selectivity of the mCEM. The results of MF 0.58 are consistent with our previous study involving AD reject water with a similar molar fraction (Kaniadakis et al., 2024). The reduced concentration of competitive monovalent cations and Mg^{2+} improved the removal of NH_4^+ using an mCEM instead of a CEM at an MF of 0.58. Finally, due to the low concentration of competing cations in MF 0.89, the mCEM showed only a slightly higher $RE_{\%}$ than the CEM.

The $E_{NH_4^+}$ for both types of membranes is shown in Fig. 6(d), (e) and (f). Results showed a higher $E_{NH_4^+}$ applying a lower MF, despite the presence of a higher electrical conductivity and equal NH_4^+ concentration. Thus, the presence of high concentrations of competitive cations relative to NH_4^+ contributed to a higher $E_{NH_4^+}$. Fig. 6(d) shows that the $E_{NH_4^+}$ at MF 0.32 was similar for both membranes until the breakpoint at a DD% of approximately 80%, when a clear difference in $E_{NH_4^+}$ was observed, with the CEM outperforming the mCEM. This steep increase in the slope was statistically significant ($p = 0.008$). Similarly, Fig. 6(e) shows that, for MF 0.58, the mCEM exhibited lower $E_{NH_4^+}$ than the CEM until an approximate $DD_{\%}$ of 80%. The increase in $E_{NH_4^+}$ ($\rho = 0.95$, $p = 0.0034$) for DD% exceeding 80% is associated with the depletion of monovalent cations and the enhanced diffusion of divalent cations into the BL, which most likely enhanced CP as discussed by previous studies (Van der Bruggen et al., 2004; Zimmermann et al., 2024). Additionally, for MF 0.89, Fig. 6(f) shows that the $E_{NH_4^+}$ using an mCEM was not significantly higher than when using a CEM, meaning that mCEM did not improve the $E_{NH_4^+}$ for MF 0.89 at any $DD_{\%}$.

3.5. *Defining the critical degree of desalination as an energy saving threshold*

Fig. 7 shows the statistically identified critical degree of desalination (CDD) for the two ED stacks determined by the change in slope of resistance for each MF. The aim was to identify the maximum $DD_{\%}$ at which the batch experiment should be terminated to yield a low resistance and high $RE_{\%}$. The CDD identified the specific $DD_{\%}$ beyond which the resistance became significantly higher from that observed before that specific $DD_{\%}$. Once the CDD was reached, the slope of the trend for all MF changed from weak linear ($R^2 = 0.2{\pm}0.02$, $\beta = -0.1{\pm}0.001$) to linear ($R^2 = 0.9{\pm}0.01$, $\beta = 0.9{\pm}0.02$). The experiment with MF 0.32 is shown in Fig. 7 (a). For the exceeded $DD_{\%}$ of 75% the resistance increased rapidly. The shift to a steep increase in resistance can be attributed to the depletion of cations in the BL (Rodrigues et al., 2022). In the case of mCEM, the higher resistance compared to CEM was attributed to the effect of the selective layer. Fig. 7 (b) shows the results for MF 0.58, where the smaller amount of competitive cations in the solution led to a shorter experimental time compared to MF 0.32. Although resistance was higher for the mCEM compared to CEM, both systems exhibited the same trend, with the resistance increasing linearly after 70% $DD_{\%}$ for the former and after 85% for the latter. Furthermore, the experiment for MF 0.89 resulted in the shortest experimental time, due to the smallest amount of total cations present (Fig. 7 (c)). Most likely, the lower concentration of divalent cations in MF 0.89 reduced the CP, and led to a shorter linear resistance trajectory. Therefore, in MF 0.89, the CDD occurred later for both membranes compared to the other MF values as shown in Table 3.

In Table 2 the results depicted in Fig. 7 are summarised, showing the beginning of the CDD correlated with the $DD_{\%}$ and $RE_{\%}$ for both membranes. At MF 0.32 and 0.58, the CDDs of mCEM occurred 20 and 30 mins earlier, respectively, than CEM. This earlier onset was accompanied by a lower $DD_{\%}$ and $RE_{\%}$. Additionally, for these two MFs, the lowest $RE_{\%}$ was 80% and the highest 86%, which fall within the range of the $RE_{\%}$ reported for recent ion-exchange and pressure driven

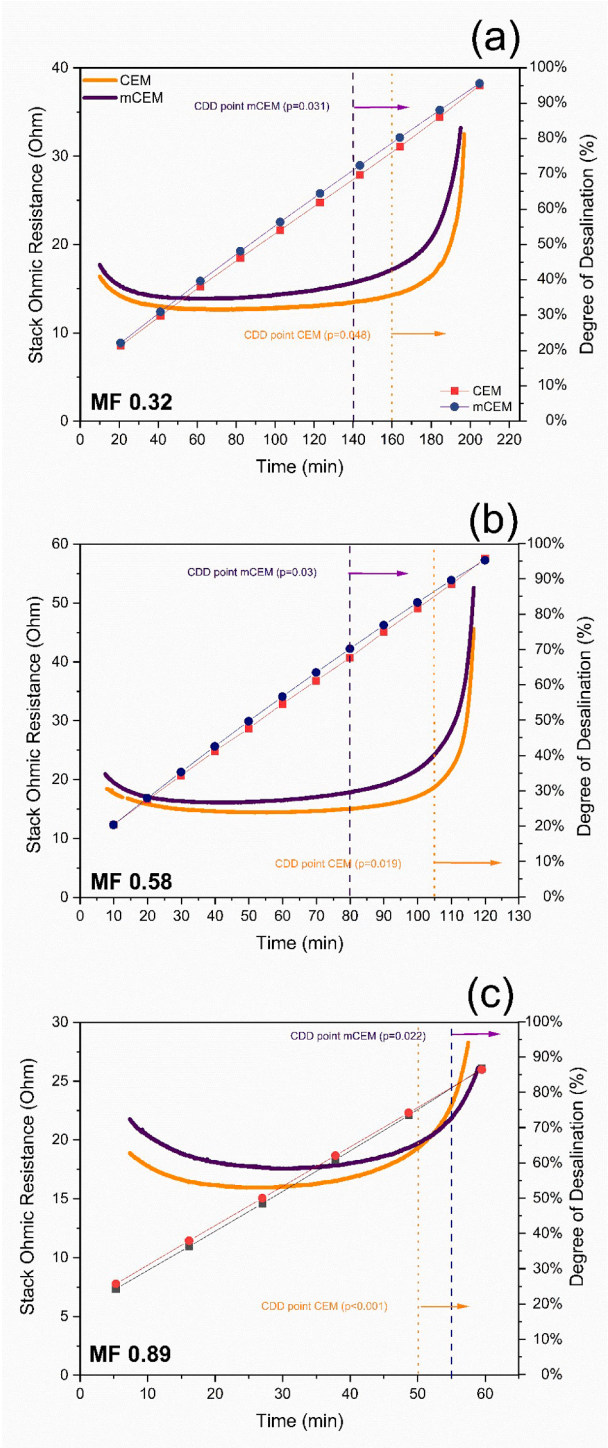

Fig. 7. The resistance of the stack in Ω (Ohms) and the degree of desalination as a function of time for CEM and mCEM at MF 0.32 (a), 0.58 (b) and 0.89 (c). The piecewise coefficient is considered statistically significant ($p < 0.05$) at a specific DD% if the null hypothesis is rejected. This hypothesis states that the total resistance after the identified CDD is not significantly different from the average resistance prior. Rejection occurred when the CDD was significantly higher.

membrane-practices (Farghali et al., 2024; Thi My Hanh et al., 2025). Furthermore, at MF 0.89, the CDD for mCEM occurred 5 mins later than that for CEM. Although the $RE_{\%}$ was higher for mCEM, the prolonged operation at a higher resistance resulted in a higher $E_{NH_4^+}$. Based on these results, it is postulated that for reject waters with an MF 0.32 to 0.58, the mCEM can contribute to a noticeable reduction in $E_{NH_4^+}$ if the operation is restricted to a $DD_{\%}$ of around 70%. This could potentially result in a delayed occurrence of scaling and energy saving in a continuous operation, if a $DD_{\%}$ of around 70% is set as a safety limit. Furthermore, for AD reject water with an MF of around 0.89, the CEM can be a more energy-efficient option than mCEM, given the shorter maximum operational time and the minimum difference in $E_{NH_4^+}$ to reach an CDD. Similarly, for a CEM a maximum $DD_{\%}$ of approximately 75% can be applied applying an MF of 0.89 to obtain a $RE_{\%}$ of at least 75% and maintain a lower resistance. The results align with the outcomes of the study conducted by (Zhang et al., 2017), where a similar value of $DD_{\%}$ at approximately 70% was identified as an optimum.

The occurrence of a CDD is therefore dependent on both the MF of the feed solution and the type of CEM employed, as summarized in Table 2. As discussed above, the transition toward CDD is associated with a change in the preferential transport behavior of monovalent to divalent cations, reflecting the progressive depletion of readily mobile monovalent charge carriers in the BL. In the case of mCEM, this depletion is reached at lower overall desalination degrees compared to conventional CEMs, indicating that transport limitations arise before the theoretical limiting-current conditions are met (Table S2). Furthermore, these limiting conditions vary with MF and are not governed entirely by the NH_4^+ concentration in the bulk, instead by the combined competitive transport of all cations present. In Table S2 the CDD times of all experiments occurred before the theoretical limiting current, indicating that limiting conditions were not yet reached despite the earlier depletion of monovalent cations. This behavior is further supported by the permeation selectivity (P_N^X) trends shown in Figures 3 and 4, where the P_N^X values of Mg^{2+} and Ca^{2+} for the mCEM increase from approximately 0.5 in the middle of the operational phase to values approaching 0.8 at the onset of CDD. This shift indicates an alteration of BL profile, consistent with intensified CP and the breakdown of the monovalent-selective transport.

For both types of membranes, the more complex composition of AD reject water led to a higher $E_{NH_4^+}$ for NH_4^+ transport despite the higher electrical conductivity in these feed waters. Regarding the $E_{NH_4^+}$ of MF 0.89 with CEM, the obtained value was halved compared to MF 0.58. It is assumed that the operational window of the CEM with MF 0.89 could surpass the CDD and still result in a competitive $E_{NH_4^+}$. For reject waters with a molar fraction of 0.89, the economic feasibility of mCEM utilization is limited. Previous studies indicate that the initial capital cost of mCEM-based stacks can be approximately 30% higher than those employing conventional CEMs (Oddonetto et al., 2024). When combined with the higher energy consumption observed under these conditions, the use of mCEMs becomes economically unattractive for this category of reject waters.

This study contributes to the identification of CDDs specific to each MF and CEM, providing a practical method for achieving the lowest feasible resistance to maximize on-site NH_4^+ $RE_{\%}$. In both batch and continuous operations, the CDD can be used to guide process control based on the desired $DD_{\%}$, without requiring real-time NH_4^+ concentration measurements and relying solely on electrical conductivity as a proxy variable. To further evaluate the relevance of the observed CDD under real-world conditions, experiments were conducted using actual AD reject water in ED, testing both membrane types. The results, presented in the Fig. 8, demonstrate that applying the CDD threshold, accounting for the type of CEMs and MF, led to an average improvement of at least 10% in $E_{NH_4^+}$ and total NH_4^+ mass recovered in the concentrate.

3.6. Sequencing batch experiments with real reject water: process control based on MF-defined threshold for critical desalination degree

The SBE runs using the CDD criterion for desalination degree control based on MF 0.58 resulted in a total of four batches, whereas the SBEs

Table 3
The CDDs identified in minutes of operation and $DD_{\%}$ for CEM and mCEM at all three MFs.

Reject water	CDD starting point (mins)		$DD_{\%}$		$RE_{\%}$		$E_{NH_4^+}$ (MJ·kgN^{-1})	
	CEM	mCEM	CEM	mCEM	CEM	mCEM	CEM	mCEM
MF = 0.32	160	140	78%	72%	71%	80%	14.2	13.6
MF = 0.58	110	80	88%	70%	75%	86%	11.2	9.4
MF = 0.89	50	55	75%	78%	79%	82%	6.2	7

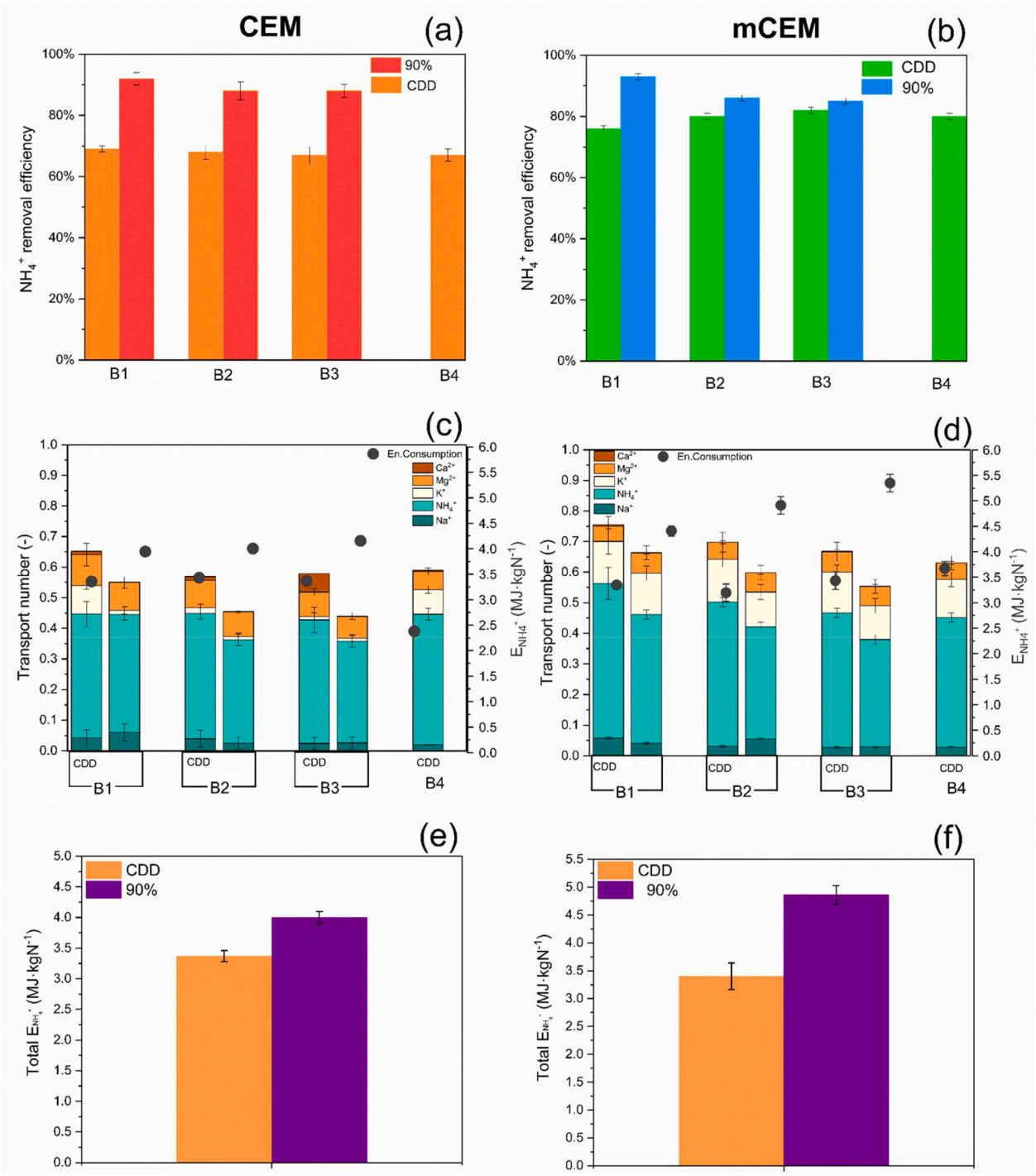

Fig. 8. The NH_4^+ removal efficiency for the SBE with CEM (a) and mCEM (b) for both operations with $DD_{\%}$ 90% and CDD. The current efficiency ($\eta_{\%}$) for all five cations per batch for both operational modes of $DD_{\%}$ presented with the $E_{NH_4^+}$ per batch for CEM (c) and mCEM (d). The total cumulative energy consumption ($E_{NH_4^+}$) in MJ kgN^{-1} of the above operational batches for CEM (e) and mCEM (f) for $DD_{\%}$ 90% and CDD.

targeting 90% desalination per batch required only three batches. Consequently, the CDD-controlled SBEs led to a higher total mass of NH_4^+ recovered in the concentrate, despite similar overall operation times. Although the NH_4^+ $RE_{\%}$ per batch was lower, the CDD-controlled SBEs treated a larger volume of reject water.

Regarding the NH_4^+ $RE_{\%}$, Fig. 8(a) shows that the difference between 90% $DD_{\%}$ and CDD control was as high as 20% for CEM. The mCEM showed a lower difference between 90% $DD_{\%}$ and CDD control, reaching values of less than 10% on average. These results show that the mCEM allows for a reduction in losses of NH_4^+ recovered when the operation is restricted by CDD control. Although the CDD control resulted in lower NH_4^+ removal, it allowed for the treatment of an additional batch to reach the target of 20 $mS{\cdot}cm^{-1}$, indicating in higher treated volume in real on-site applications.

Fig. 8(c) and (d) shows that the CDD control operation improved the $\eta_{\%}$ for NH_4^+ compared to 90% $DD_{\%}$ for both types of membranes, similar to the findings using synthetic MFs. Moreover, the mCEM enhanced the transport of NH_4^+ and reduced the transport of divalent cations compared to CEM.

Overall, the CDD control resulted in a lower $E_{NH_4^+}$ per batch and total $E_{NH_4^+}$ compared to $DD_{\%}$ of 90% for both membrane stacks (Fig. 8(e),(f)). Thus, the additional results using real AD reject water indicated the usability of the proposed strategy for field scenarios, improving the overall ED performance, enhancing NH_4^+ transport, and reducing the $E_{NH_4^+}$ with at least 10%.

3.7. Future outlook

Rodrigues et al. (2017) showed that a higher load ratio of applied current density over charge of NH_4^+ leads to co-transport of other cations if present in the solution. Therefore, in an NH_4^+-rich wastewater source it is challenging to predict the exact $\eta_{\%}$ of NH_4^+ based on L_N as other cations take part in the transport (Kuntke et al., 2018). As demonstrated in Table S1, NH_4^+ is not the only species contributing to the current density, therefore, applying an identical L_N across all three molar fractions results in performance discrepancies. Therefore, the $DD_{\%}$ could be applied as an approximation and practical alternative to this uncertainty for on-site treatment of AD reject water with ED. In this study, the ED operation was in batch mode and the feed waters did not contain any organic compounds. Thus, future work should focus on a continuous operation applied on various MF in real AD reject water to determine the impact of organic fouling and scaling in resistance while aiming at steady CDD conditions. Finally, to further assess the practical viability of mCEMs, a comprehensive techno-economic assessment should be conducted, including payback time analysis to account for their higher capital expenditure.

4. Conclusions

This study demonstrates the influence of feed water cation composition and membrane selectivity on ammonium (NH_4^+) transport in electrodialysis. Across all tested molar fractions (MF 0.32, 0.58, and 0.89), the monovalent-selective cation exchange membrane (mCEM) consistently outperformed the conventional CEM in terms of NH_4^+ current efficiency ($\eta_{\%}$) and removal efficiency ($RE_{\%}$), particularly at the intermediate molar fraction (MF 0.58). The application of a "degree of desalination" threshold to avoid the occurrence of CDD based on membrane type and molar fraction is recommended to improve the energy consumption and current efficiency of electrodialysis.

- The mCEMs are optimal for reject waters of MF 0.32–0.58: The mCEM consistently outperformed the CEM in all experiments regarding perm-selectivity (P_N^X) in favour of NH_4^+. Specifically, the mCEM effectively reduced the transport of Ca^{2+} and Mg^{2+}, achieving a P_N^X below 1 for every MF consistently. In contrast, the CEM showed preferential selectivity for Ca^{2+} and Mg^{2+} over NH_4^+ across every MF. The competitive transport of K^+ in MF 0.32 resulted in the lowest $\eta_{\%}$ of NH_4^+. The $E_{NH_4^+}$ for both types of membranes was reduced for high molar fractions. The $E_{NH_4^+}$ of mCEM for MF 0.32 was similar to that of CEM until a $DD_{\%}$ of approximately 80%. Meaning that the mCEM improved NH_4^+ perm-selectivity for the same energy cost. The mCEM reduced the $E_{NH_4^+}$ for MF 0.58 compared to CEM but resulted to slightly higher $E_{NH_4^+}$ in MF 0.89. Until the occurrence of CDD, the mCEM achieved higher removal efficiency than CEM for MF 0.32 and 0.58, but only slightly higher for 0.89.
- Standard CEMs are preferable at higher molar fractions: The improved perm-selectivity of mCEM comes at the cost of higher resistance and intensified CP, which may compromise the removal efficiency for $DD_{\%}$ exceeding 75%−80%, particularly at MF 0.32 and 0.58. Therefore, the use of mCEM may not offer a significant advantage in reducing $E_{NH_4^+}$ for reject waters with MF around 0.89. In fact, the conventional CEM at MF 0.89 resulted in nearly a 50% reduction in $E_{NH_4^+}$ compared to a MF of 0.58 and 0.32.
- A critical degree of desalination can be applied for ED process control: The controlled electrodialysis operation with the applied CDD criterion, based on the molar fraction, improved the overall performance in terms of NH_4^+ current efficiency and energy consumption, compared to 90% aiming NH_4^+ removal. Therefore, the CDD-controlled operation offers a practical solution for on-site-process-control of real AD reject waters based on their MF composition when targeting NH_4^+ removal.

CRediT authorship contribution statement

Iosif Kaniadakis: Writing – original draft, Visualization, Validation, Supervision, Methodology, Investigation, Conceptualization. **Zhenqiu Yang:** Validation, Investigation, Data curation, Conceptualization. **Marianna Papadopoulou:** Validation, Investigation, Data curation, Conceptualization. **Jules B. van Lier:** Writing – review & editing, Supervision, Project administration, Funding acquisition. **Henri Spanjers:** Writing – review & editing, Supervision, Resources.

Declaration of competing interest

The authors declare the following financial interests/personal relationships which may be considered as potential competing interests:

Iosif Kaniadakis reports financial support was provided by Delft University of Technology. If there are other authors, they declare that they have no known competing financial interests or personal relationships that could have appeared to influence the work reported in this paper.

Acknowledgements

This work was financially supported by the Netherlands Enterprise Agency, also known as Rijksdienst voor Ondernemend Nederland (RVO), through the Demonstration of Energy Innovation (DEI+) grant CEI120070. Additionally, the research received a contribution from the Foundation for Applied Water Research (STOWA). The authors would like to acknowledge the valuable contributions of the following project partners: Blue-Tec BV, W&F Technologies BV, i3 Innovative Technologies BV, Waterschapsbedrijf Limburg, Waterschap Amstel, Gooi en Vecht.

Supplementary materials

Supplementary material associated with this article can be found, in the online version, at doi:10.1016/j.watres.2026.125770.

Data availability

Data will be made available on request.

References

Ahdab, Y.D., Schücking, G., Rehman, D., Lienhard, J.H., 2021. Treatment of greenhouse wastewater for reuse or disposal using monovalent selective electrodialysis. Desalination 507, 115037. https://doi.org/10.1016/j.desal.2021.115037.

Al-Amshawee, S., Yunus, M.Y.B.M., Azoddein, A.A.M., Hassell, D.G., Dakhil, I.H., Hasan, H.A., 2020. Electrodialysis desalination for water and wastewater: a review. Chem. Eng. J. 380, 122231. https://doi.org/10.1016/j.cej.2019.122231.

Bao, X., She, Q., Long, W., Wu, Q., 2021. Ammonium ultra-selective membranes for wastewater treatment and nutrient enrichment: interplay of surface charge and hydrophilicity on fouling propensity and ammonium rejection. Water Res. 190, 116678. https://doi.org/10.1016/j.watres.2020.116678.

Chen, M., Ma, J., Wang, Z., Zhang, X., Wu, Z., 2017. Insights into iron induced fouling of ion-exchange membranes revealed by a quartz crystal microbalance with dissipation monitoring. RSC Adv. 7, 36555–36561. https://doi.org/10.1039/C7RA05510B.

Deng, Z., van Linden, N., Guillen, E., Spanjers, H., van Lier, J.B., 2021. Recovery and applications of ammoniacal nitrogen from nitrogen-loaded residual streams: a review. J. Environ. Manag. 295, 113096. https://doi.org/10.1016/j.jenvman.2021.113096.

El-Qelish, M., Mahmoud, M., 2022. Overcoming organic matter limitation enables high nutrient recovery from sewage sludge reject water in a self-powered microbial nutrient recovery cell. Sci. Total Environ. 802, 149851. https://doi.org/10.1016/j.scitotenv.2021.149851.

Farghali, M., Chen, Z., Osman, A.I., Ali, I.M., Hassan, D., Ihara, I., Rooney, D.W., Yap, P. S., 2024. Strategies for ammonia recovery from wastewater: a review. Environ. Chem. Lett. 22, 2699–2751. https://doi.org/10.1007/s10311-024-01768-6.

Ferrari, F., Pijuan, M., Molenaar, S., Duinslaeger, N., Sleutels, T., Kuntke, P., Radjenovic, J., 2022. Ammonia recovery from anaerobic digester centrate using onsite pilot scale bipolar membrane electrodialysis coupled to membrane stripping. Water Res. 218, 118504. https://doi.org/10.1016/J.WATRES.2022.118504.

Firdaous, L., Malériat, J.P., Schlumpf, J.P., Quéméneur, F., 2007. Transfer of monovalent and divalent cations in salt solutions by electrodialysis. Sep. Sci. Technol. 42, 931–948. https://doi.org/10.1080/01496390701206413.

Ippersiel, D., Mondor, M., Lamarche, F., Tremblay, F., Dubreuil, J., Masse, L., 2012. Nitrogen potential recovery and concentration of ammonia from swine manure using electrodialysis coupled with air stripping. J. Environ. Manag. 95, S165–S169. https://doi.org/10.1016/J.JENVMAN.2011.05.026.

Kaniadakis, I., van Lier, J.B., Spanjers, H., 2024. Removal of total ammoniacal nitrogen from reject water through selective electrodialysis reversal and bipolar electrodialysis. Chem. Eng. J. 493, 152613. https://doi.org/10.1016/j.cej.2024.152613.

Kim, Y., Walker, W.S., Lawler, D.F., 2012. Competitive separation of di- vs. mono-valent cations in electrodialysis: effects of the boundary layer properties. Water Res. 46, 2042–2056. https://doi.org/10.1016/j.watres.2012.01.004.

Kim, Y., Walker, W.S., Lawler, D.F., 2011. Electrodialysis with spacers: effects of variation and correlation of boundary layer thickness. Desalination 274, 54–63. https://doi.org/10.1016/j.desal.2011.01.076.

Koskue, V., Freguia, S., Ledezma, P., Kokko, M., 2021a. Efficient nitrogen removal and recovery from real digested sewage sludge reject water through electroconcentration. J. Environ. Chem. Eng. 9, 106286. https://doi.org/10.1016/j.jece.2021.106286.

Koskue, V., Rinta-Kanto, J.M., Freguia, S., Ledezma, P., Kokko, M., 2021b. Optimising nitrogen recovery from reject water in a 3-chamber bioelectroconcentration cell. Sep. Purif. Technol. 264, 118428. https://doi.org/10.1016/j.seppur.2021.118428.

Kuntke, P., Rodrigues, M., Sleutels, T., Saakes, M., Hamelers, H.V.M., Buisman, C.J.N., 2018. Energy-efficient ammonia recovery in an up-scaled hydrogen gas recycling electrochemical system. ACS Sustain. Chem. Eng. 6, 7638–7644. https://doi.org/10.1021/acssuschemeng.8b00457.

Lambert, J., Avila-Rodriguez, M., Durand, G., Rakib, M., 2006. Separation of sodium ions from trivalent chromium by electrodialysis using monovalent cation selective membranes. J. Memb. Sci. 280, 219–225. https://doi.org/10.1016/J.MEMSCI.2006.01.021.

Meng, J., Shi, X., Wang, S., Hu, Z., Koseoglu-Imer, D.Y., Lens, P.N.L., Zhan, X., 2024. Application of electrodialysis technology in nutrient recovery from wastewater: a review. J. Water Process. Eng. 65, 105855. https://doi.org/10.1016/j.jwpe.2024.105855.

Mondor, M., Masse, L., Ippersiel, D., Lamarche, F., Massé, D.I., 2008. Use of electrodialysis and reverse osmosis for the recovery and concentration of ammonia from swine manure. Bioresour. Technol. 99, 7363–7368. https://doi.org/10.1016/J.BIORTECH.2006.12.039.

Myllymäki, P., Pesonen, J., Nurmesniemi, E.-T., Romar, H., Tynjälä, P., Hu, T., Lassi, U., 2020. The use of industrial waste materials for the simultaneous removal of ammonium nitrogen and phosphate from the Anaerobic digestion reject water. Waste Biomass Valorizat. 11, 4013–4024. https://doi.org/10.1007/s12649-019-00724-8.

Oddonetto, T.L., Deemer, E., Lugo, A., Cappelle, M., Xu, P., Santiago, I., Walker, W.S., 2024. Assessment of salt-free electrodialysis metathesis: a novel process for brine management in brackish water desalination using monovalent selective ion exchange membranes. Desalination 592, 118160. https://doi.org/10.1016/j.desal.2024.118160.

Pavez-Jara, J.A., van Lier, J.B., de Kreuk, M.K., 2023. Effects of thermal hydrolysis process-generated melanoidins on partial nitritation/anammox in full-scale installations treating waste activated sludge. J. Clean. Prod. 432, 139767. https://doi.org/10.1016/j.jclepro.2023.139767.

Proskynitopoulou, V., Vourros, A., Dimopoulos Toursidis, P., Garagounis, I., Lorentzou, S., Bampaou, M., Plakas, K., Zouboulis, A., Panopoulos, K., 2024. Selective electrodialysis for nutrient recovery and pharmaceutical removal from liquid digestate: pilot-scale investigation and potential fertilizer production. Bioresour. Technol. 412, 131386. https://doi.org/10.1016/j.biortech.2024.131386.

Rodrigues, M., Molenaar, S., Barbosa, J., Sleutels, T., Hamelers, H.V.M., Buisman, C.J.N., Kuntke, P., 2023. Effluent pH correlates with electrochemical nitrogen recovery efficiency at pilot scale operation. Sep. Purif. Technol. 306, 122602. https://doi.org/10.1016/J.SEPPUR.2022.122602.

Rodrigues, M., Sleutels, T., Kuntke, P., Buisman, C.J.N., Hamelers, H.V.M., 2022. Effects of current on the membrane and boundary layer selectivity in electrochemical systems designed for nutrient recovery. ACS Sustain. Chem. Eng. 10, 9411–9418. https://doi.org/10.1021/acssuschemeng.2c01764.

Rodrigues, M., Sleutels, T., Kuntke, P., Hoekstra, D., ter Heijne, A., Buisman, C.J.N., Hamelers, H.V.M., 2020. Exploiting donnan dialysis to enhance ammonia recovery in an electrochemical system. Chem. Eng. J. 395, 125143. https://doi.org/10.1016/J.CEJ.2020.125143.

Rodríguez Arredondo, M., Kuntke, P., ter Heijne, A., Buisman, C.J., 2019. The concept of load ratio applied to bioelectrochemical systems for ammonia recovery. J. Chem. Technol. Biotechnol. 94, 2055–2061. https://doi.org/10.1002/jctb.5992.

Rodríguez Arredondo, M., Kuntke, P., ter Heijne, A., Hamelers, H.V.M., Buisman, C.J.N., 2017. Load ratio determines the ammonia recovery and energy input of an electrochemical system. Water Res. 111, 330–337. https://doi.org/10.1016/J.WATRES.2016.12.051.

Roghmans, F., Evdochenko, E., Martí-Calatayud, M.C., Garthe, M., Tiwari, R., Walther, A., Wessling, M., 2020. On the permselectivity of cation-exchange membranes bearing an ion selective coating. J. Memb. Sci. 600, 117854. https://doi.org/10.1016/j.memsci.2020.117854.

Sadrzadeh, M., Razmi, A., Mohammadi, T., 2007. Separation of monovalent, divalent and trivalent ions from wastewater at various operating conditions using electrodialysis. Desalination 205, 53–61. https://doi.org/10.1016/j.desal.2006.04.039.

Shaddel, S., Grini, T., Andreassen, J.P., Østerhus, S.W., Ucar, S., 2020a. Crystallization kinetics and growth of struvite crystals by seawater versus magnesium chloride as magnesium source: towards enhancing sustainability and economics of struvite crystallization. Chemosphere 256, 126968. https://doi.org/10.1016/j.chemosphere.2020.126968.

Shaddel, S., Grini, T., Ucar, S., Azrague, K., Andreassen, J.P., Østerhus, S.W., 2020b. Struvite crystallization by using raw seawater: improving economics and environmental footprint while maintaining phosphorus recovery and product quality. Water Res. 173, 115572. https://doi.org/10.1016/j.watres.2020.115572.

Shocron, A.N., Monat, L., Januszewski, B., Dykstra, J.E., Elimelech, M., Nir, O., 2025. Ion selectivity in brackish groundwater desalination by electrodialysis: experiments and theory. J. Memb. Sci. 719, 123668. https://doi.org/10.1016/j.memsci.2024.123668.

Strathmann, H., 2010. Electrodialysis, a mature technology with a multitude of new applications. Desalination 264, 268–288. https://doi.org/10.1016/J.DESAL.2010.04.069.

Tanaka, Y., 2003. Concentration polarization in ion-exchange membrane electrodialysis—The events arising in a flowing solution in a desalting cell. J. Memb. Sci. 216, 149–164. https://doi.org/10.1016/S0376-7388(03)00067-X.

Thi My Hanh, N., Hong Van, N., Thi Minh Trang, P., 2025. Ammonium recovering from domestic wastewater toward circular economy: a short review. Desalination Water Treat. 321, 100906. https://doi.org/10.1016/j.dwt.2024.100906.

Van der Bruggen, B., Koninckx, A., Vandecasteele, C., 2004. Separation of monovalent and divalent ions from aqueous solution by electrodialysis and nanofiltration. Water Res. 38, 1347–1353. https://doi.org/10.1016/j.watres.2003.11.008.

van Linden, N., Bandinu, G.L., Vermaas, D.A., Spanjers, H., van Lier, J.B., 2020. Bipolar membrane electrodialysis for energetically competitive ammonium removal and dissolved ammonia production. J. Clean. Prod. 259, 120788. https://doi.org/10.1016/j.jclepro.2020.120788.

van Linden, N., Spanjers, H., van Lier, J.B., 2019. Application of dynamic current density for increased concentration factors and reduced energy consumption for concentrating ammonium by electrodialysis. Water Res. 163, 114856. https://doi.org/10.1016/j.watres.2019.114856.

Vermaas, D.A., Saakes, M., Nijmeijer, K., 2014. Enhanced mixing in the diffusive boundary layer for energy generation in reverse electrodialysis. J. Memb. Sci. 453, 312–319. https://doi.org/10.1016/J.MEMSCI.2013.11.005.

Wang, R., Lin, S., 2024. Membrane design principles for ion-selective electrodialysis: an analysis for Li/Mg separation. Environ. Sci. Technol. https://doi.org/10.1021/acs.est.3c08956.

Ward, A.J., Arola, K., Thompson Brewster, E., Mehta, C.M., Batstone, D.J., 2018. Nutrient recovery from wastewater through pilot scale electrodialysis. Water Res. 135, 57–65. https://doi.org/10.1016/J.WATRES.2018.02.021.

Xiang, S., Liu, Y., Zhang, G., Ruan, R., Wang, Y., Wu, X., Zheng, H., Zhang, Q., Cao, L., 2020. New progress of ammonia recovery during ammonia nitrogen removal from various wastewaters. World J. Microbiol. Biotechnol. 36, 144. https://doi.org/10.1007/s11274-020-02921-3.

Xiao, H., Pan, F., Huang, F., Zhu, H., Wu, Q., 2023. Three-segmented counterflow pilot-scale electrodialysis for ammonia and potassium treatment in liquid anaerobic digestate: a trade-off among advanced ion removal, nutrients concentration limitation, and energy consumption. Chem. Eng. J. 472, 144941. https://doi.org/10.1016/j.cej.2023.144941.

Yang, D., Liu, H., She, Q., 2023. Mixed cation transport behaviours in electrodialysis during simultaneous ammonium enrichment and wastewater desalination. Desalination 545, 116155. https://doi.org/10.1016/j.desal.2022.116155.

Ye, Z.-L., Ghyselbrecht, K., Monballiu, A., Rottiers, T., Sansen, B., Pinoy, L., Meesschaert, B., 2018. Fractionating magnesium ion from seawater for struvite recovery using electrodialysis with monovalent selective membranes. Chemosphere 210, 867–876. https://doi.org/10.1016/j.chemosphere.2018.07.078.

Zhang, W., Miao, M., Pan, J., Sotto, A., Shen, J., Gao, C., der Bruggen, B.V., 2017. Separation of divalent ions from seawater concentrate to enhance the purity of coarse salt by electrodialysis with monovalent-selective membranes. Desalination 411, 28–37. https://doi.org/10.1016/j.desal.2017.02.008.

Zimmermann, P., Wahl, K., Tekinalp, Ö., Solberg, S.B.B., Deng, L., Wilhelmsen, Ø., Burheim, O.S., 2024. Selective recovery of silver ions from copper-contaminated effluents using electrodialysis. Desalination 572, 117108. https://doi.org/10.1016/j.desal.2023.117108.